New Journal of Physics
The open access journal at the forefront of physics

Deutsche Physikalische Gesellschaft DPG IOP Institute of Physics

PAPER • OPEN ACCESS

Carrier-envelope phase controlled isolated attosecond pulses in the nm wavelength range, based on coherent nonlinear Thomson-backscattering

To cite this article: Szabolcs Hack *et al* 2018 *New J. Phys.* **20** 073043

New Journal of Physics
The open access journal at the forefront of physics

Deutsche Physikalische Gesellschaft DPG
IOP Institute of Physics

Published in partnership with: Deutsche Physikalische Gesellschaft and the Institute of Physics

OPEN ACCESS

RECEIVED
10 April 2018

REVISED
14 June 2018

ACCEPTED FOR PUBLICATION
11 July 2018

PUBLISHED
24 July 2018

PAPER

Carrier-envelope phase controlled isolated attosecond pulses in the nm wavelength range, based on coherent nonlinear Thomson-backscattering

Szabolcs Hack[1], **Sándor Varró**[1,2] **and Attila Czirják**[1,3]

[1] ELI-ALPS, ELI-HU Non-Profit Ltd., H-6720 Szeged, Dugonics tér 13, Hungary
[2] Wigner Research Center for Physics, SZFI, H-1525 Budapest, PO Box 49, Hungary
[3] Department of Theoretical Physics, University of Szeged, H-6720 Szeged, Tisza L. krt. 84-86, Hungary

E-mail: czirjak@physx.u-szeged.hu

Keywords: attosecond pulses, ultrafast phenomena, backscattering, extreme ultraviolet, soft x-rays

Abstract

A proposal for a novel source of isolated attosecond XUV—soft x-ray pulses with a well controlled carrier-envelope phase difference (CEP) is presented in the framework of nonlinear Thomson-backscattering. Based on the analytic solution of the Newton–Lorentz equations, the motion of a relativistic electron is calculated explicitly, for head-on collision with an intense fs laser pulse. By using the received formulas, the collective spectrum and the corresponding temporal shape of the radiation emitted by a mono-energetic electron bunch can be easily computed. For certain suitable and realistic parameters, single-cycle isolated pulses of ca. 20 as length are predicted in the XUV—soft x-ray spectral range, including the 2.33–4.37 nm water window. According to our analysis, the generated almost linearly polarized beam is extremely well collimated around the initial velocity of the electron bunch, with considerable intensity and with its CEP locked to that of the fs laser pulse.

1. Introduction

Isolated attosecond XUV pulses allow us to investigate the real time electron dynamics in atoms, molecules and solids experimentally [1]. It is well-known, that the carrier-envelope phase difference (CEP) of the femtosecond laser pulse, involved in most of these pioneering experiments, affects various processes [2–4] in atomic or molecular systems on this time scale. Recently, it was predicted that it is also crucial to control the CEP of the attosecond pulses in these pump–probe experiments [5–8].

Currently, the established way to generate attosecond XUV pulses is based on high-order harmonic generation in noble gas samples [9], which has its limitations both in pulse length and intensity. In this contribution, we are going to show that nonlinear Thomson-backscattering provides a very promising method to generate an isolated attosecond pulse with its CEP determined by the CEP of the driving fs laser pulse.

Nonlinear Thomson-backscattering of a high intensity laser pulse on a bunch of relativistic electrons [10] has long been used as a source of x- and gamma-ray radiation [11, 12], usually with an emphasis on monochromatic features [13, 14] or producing pulses of ps or fs length [15, 16]. For a tutorial paper providing asymptotic formulas for single electron spectra see [17], for a review with broad coverage of the experimental developments see e.g. [18] and references therein. To our best knowledge, results on attosecond (and even shorter) pulses or pulse trains based on this process were published only in the hard x- and gamma-ray spectral range [19–22], except for our previous work which merely mentioned the possibility of attosecond pulse generation in a similar scenario, assuming spectral filtering [23].

The generation of electron bunches suitable for nonlinear Thomson-backscattering (i.e. fs and sub-fs pulse length, low emittance, sufficient density and energy, small enough energy spread) was promoted by pioneering experiments [24, 25] and enlightening simulation results [26] over the past two decades [18, 27]. More recent developments include the utilization of velocity bunching to generate an electron bunch with pC charge in the

MeV energy range [21], recently with already sub-10 fs pulse length [28, 29], and a work on bunch compressing [30] predicting electron bunches of 2 as duration and 5.2 MeV energy. Several research groups on laser-wakefield acceleration reported about quasi-mono-energetic, fs or sub-fs electron bunch trains [31–33], and one group reported about a single (isolated) bunch [34], having 10–100 pC charge (i.e. 10^7–10^8 electrons) and an energy in the few to few hundred MeV range. In addition we note that beyond the classical means to produce attosecond electron bunches, there is a possibility for generating such bunches by quantum interference, as has been shown in [35], though in the nonrelativistic regime. At relativistic incoming laser intensities, on the other hand, such bunches can also produce very high-order harmonics which may be useful, for instance, in soft x-ray imaging techniques.

In this paper, based on but largely extending our earlier works [23, 36], we investigate in detail the radiation of a realistic attobunch of electrons due to a near infrared (NIR) fs laser pulse in the 10^{18}–10^{19} W cm^{-2} intensity range. First, we explicitly give the analytic solution of the Newton–Lorentz equations for an electron moving in a plane wave for a laser pulse with sine-squared envelope, having an arbitrary number of cycles and CEP. Using this result, we compute the radiation emitted by a bunch of N electrons, both in frequency and in time domain. We analyze the temporal and spatial profile of the resulting isolated attosecond pulse, and we highlight its remarkable properties regarding the dependence of its CEP and intensity on those of the driving laser pulse.

2. Analytic solution of the electron's equation of motion

We assume that the laser pulse propagates in the z direction and it is linearly polarized along the x direction. First, we consider one electron only, which moves initially in the $-z$ direction, i.e. we investigate a head-on collision. We model the electric field of the laser pulse, $\mathbf{E} = (E_x, 0, 0)$, with the usual sine-squared envelope:

$$E_x(\theta) = E_0 \sin^2\left(\frac{\omega_L \theta}{2n_c}\right)\cos(\omega_L\theta - \varphi_0), \tag{1}$$

where E_0 is the amplitude, ω_L is the angular frequency, n_c is the number of optical cycles in the pulse, φ_0 is the CEP and $\theta = t - \mathbf{n}_L\cdot\mathbf{r}/c$ is the wave argument of the laser pulse at position $\mathbf{r}$, with $\mathbf{n}_L$ denoting the unit vector pointing in the propagation direction. We neglect the effects of the transverse profile of the laser beam, in order to have the advantage of analytic treatment. For detailed numerical investigations of the effects of the transverse beam profile see [37–39].

The Newton–Lorentz equations govern the motion of a relativistic electron with charge e and mass m during its interaction with the laser pulse as

$$m\frac{\mathrm{d}\mathbf{u}}{\mathrm{d}\tau} = \frac{e}{c}[u^0\mathbf{E}(\theta) + \mathbf{n}_L(\mathbf{u}\cdot\mathbf{E}(\theta)) - \mathbf{E}(\theta)(\mathbf{n}_L\cdot\mathbf{u})], \tag{2}$$

$$m\frac{\mathrm{d}u^0}{\mathrm{d}\tau} = \frac{e}{c}\mathbf{E}(\theta)\cdot\mathbf{u}, \tag{3}$$

where $(u^0, \mathbf{u}) = (\gamma c, \gamma\mathbf{v})$ is the four-velocity, $\gamma \equiv (1 - |\mathbf{v}|^2/c^2)^{-1/2}$ is the Lorentz factor and $\mathrm{d}\tau = \mathrm{d}t/\gamma$ is the proper time element of the electron. In (3) we have made use of the $\mathbf{B} = \mathbf{n}_L \times \mathbf{E}/c$, connecting the magnetic induction and the electric field strength of a plane wave. As it is well-known, the equations of motion (2), (3) have a general analytic solution due to the following linear relation between the proper time of the electron and wave argument [40–42]:

$$u^0 - u^3 = \frac{\mathrm{d}}{\mathrm{d}\tau}(ct - z) = c\frac{\mathrm{d}\theta}{\mathrm{d}\tau} = \alpha c, \tag{4}$$

where $\alpha = \gamma(1 - v_z/c)$ is a dimensionless constant of motion depending on the initial conditions of the electron only. We have determined the solution of (2), (3) for the pulse shape (1) explicitly, which reads as

$$x(\theta) = x(\theta_0) + V_{x_0}(\theta - \theta_0) + c\omega(\theta), \tag{5}$$

$$y(\theta) = y(\theta_0) + V_{y_0}(\theta - \theta_0), \tag{6}$$

$$z(\theta) = z(\theta_0) + \lambda(\theta - \theta_0) + V_{x_0}\omega(\theta) + \delta(\theta). \tag{7}$$

The $t(\theta)$ component has the same functional form as the $z(\theta)$ according to equation (4), they differ in the initial conditions only. We introduced above the following quantities, having the dimension of velocity:

$$V_{x_0} = \alpha^{-1}u^1(\theta_0) + cf(\theta_0), \tag{8}$$

$$V_{y_0} = \alpha^{-1}u^2(\theta_0), \tag{9}$$

$$V_{z_0} = \alpha^{-1}u^3(\theta_0) + g(\theta_0) + h(\theta_0) + l(\theta_0), \tag{10}$$

with

$$f(\theta) = \sum_{j=-1}^{1} \left(-\frac{1}{2}\right)^{1+|j|} \frac{\nu\, n_c}{n_c + j} \sin\left(\frac{n_c + j}{n_c}\theta\omega_L + \varphi_0\right), \tag{11}$$

$$g(\theta) = -\frac{c\nu^2}{2}\frac{n_c^2}{n_c^2 - 1}\sum_{j=1}^{2}\left(-\frac{1}{4}\right)^j \cos\left(j\frac{\theta\omega_L}{n_c}\right), \tag{12}$$

$$h(\theta) = \frac{c\nu^2}{32}\frac{3n_c^2 - 2}{n_c^2 - 1}\cos\left(2(\theta\omega_L + \varphi_0)\right), \tag{13}$$

$$l(\theta) = \frac{c\nu^2}{4}\sum_{k=1}^{2}\sum_{j=\{-1,1\}}\left(-\frac{n_c}{4(n_c + j)}\right)\cos\left(\frac{2n_c + kj}{n_c}\theta\omega_L + 2\varphi_0\right), \tag{14}$$

where $\nu = |e|\, E_0/mc\omega_L\alpha = a_0/\alpha$ is the effective intensity parameter, and $a_0 = 8.5 \times 10^{-10}\lambda(\mu\text{m})\sqrt{I_0(\text{W cm}^{-2})}$ denotes the dimensionless vector potential (the usual intensity parameter). The $\omega(\theta)$ is an oscillating function defined as

$$\omega(\theta) = -\int_{\theta_0}^{\theta} f(\theta')\mathrm{d}\theta', \tag{15}$$

making the $c\omega(\theta)$ to be the dominating term in $x(\theta)$. The λ is a constant depending on the initial values only:

$$\lambda = V_{z_0} + V_{x_0} f(\theta_0). \tag{16}$$

In $z(\theta)$, the λ is the most dominant term because V_{z_0} is larger than all the other terms for a relativistic electron moving in the z direction. The $\delta(\theta)$ is the well-known trajectory with systematic drift caused by the classical radiation pressure:

$$\delta(\theta) = -\int_{\theta_0}^{\theta}[g(\theta') + h(\theta') + l(\theta')]\mathrm{d}\theta'. \tag{17}$$

Since f, g, h, l are linear combinations of simple trigonometric functions of θ, the explicit formulas for ω and δ can be easily obtained.

Due to the use of the wave argument θ, the specification of the initial values for the solution (5)–(7) requires some attention [23, 36]. The interaction of an electron with the laser pulse starts if $\theta = \theta_0$ and it ends if $\theta = \theta_1$, i.e. these are specified on a light-like hyper-surface. This means, that one has to transform the usual initial conditions, which are valid in a lab-frame (i.e. on a space-like hyper-surface), to the light-like hyper-surface. Ignoring this important step leads to false peaks in the calculated spectrum, as we demonstrated it in [23].

3. Emitted radiation spectra

Now we proceed to evaluate the spectrum of radiation emitted by an electron, moving according to the solution (5)–(7). We specify an almost single-cycle sine laser pulse by setting $n_c = 3$ and $\varphi_0 = \pi/2$, with a carrier wavelength of $\lambda_L = 800$ nm and a dimensionless vector potential of $a_0 = 1$, corresponding to a peak electric field of ca. 4×10^{12} V m^{-1}. (Note that this terminology about the pulse length (FWHM) measured in the number of cycles is commonly used in the laser physics community, although the laser pulse has 3 optical cycles under the envelope function, see inset on figure 7.) The emitted radiation field of an electron in the far-field is given by the following formula [43]:

$$\mathbf{E}_1(\omega) = \frac{e}{c}\frac{\mathrm{e}^{\mathrm{i}\omega R_0/c}}{4\pi\epsilon_0 R_0}\int_{-\infty}^{\infty}\frac{\mathbf{n}\times[(\mathbf{n} - \beta)\times\dot{\beta}]}{(1 - \mathbf{n}\cdot\beta)^2}\mathrm{e}^{\mathrm{i}\omega(t - \mathbf{n}\cdot\mathbf{r}(t)/c)}\mathrm{d}t, \tag{18}$$

where R_0 is the distance of the observation point, $\mathbf{n}$ is the unit vector pointing towards the observer, $\beta = \mathbf{v}/c$ and $\dot{\beta}$ are the normalized velocity and acceleration, respectively. Here we note that in case of a charge interacting with a fs laser pulse it is essential to use (18) which includes also the end point terms that are usually neglected [44].

By changing the integration variable from t to θ, we can use the analytic trajectories (5)–(7) for calculating the emitted radiation. The resulting single electron radiation spectrum is shown in figure 1 for two selected values of the initial Lorentz factor γ_0, along the directions $\mathbf{n}$ in the x–z plane defined by the indicated polar angles ϑ (i.e. along and very close to the direction of the electron's initial velocity at 180°). In order to compare the angle dependence to the well-known $1/\gamma_0$ divergence of the radiation generated by a long laser pulse, we chose $\vartheta = 174.3°$ and $\vartheta = 177.1°$ in the case of $\gamma_0 = 10$, and $\vartheta = 176.2°$ and $\vartheta = 178.1°$ in the case of $\gamma_0 = 15$, corresponding to polar angles $1/\gamma_0$ and $1/2\gamma_0$, respectively. We see that these single electron spectra are more sensitive with respect to the change of ϑ than those generated by a long laser pulse [10, 45–47], for both of these values of γ_0. The spectra along the polar angles $\vartheta = 179.9°$ and $\vartheta = 179.8°$ in the case of $\gamma_0 = 10$, and

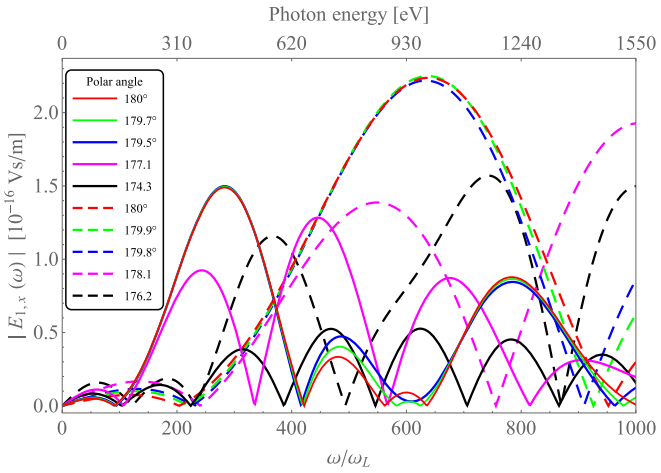

Figure 1. Nonlinear Thomson-backscattering spectra of a single electron in head-on collision with a single-cycle laser pulse of sine-squared envelope, equation (18). We plot the spectra of the dominant x-component of the electric field for $\gamma_0 = 10$ (solid lines) and for $\gamma_0 = 15$ (dashed lines), along the propagation directions in the x–z plane, specified by the polar angles in the legend. ($E_{1,x}(\omega)$ is at least 1000 times larger than $E_{1,y}(\omega)$ or $E_{1,z}(\omega)$.) Other parameters: $\lambda_L = 800$ nm, $n_c = 3$, $a_0 = 1$, $R_0 = 2$ m.

$\vartheta = 179.7°$ and $\vartheta = 179.5°$ in the case of $\gamma_0 = 15$, i.e. extremely close to 180°, are suggested by the collective spectra along the same polar angles in figures 3 and 4 since these turn out to be characteristic to the divergence of the collective radiation.

The spectra and their angular dependence are similar for the two values of γ_0, although for $\gamma_0 = 15$ the spectral peaks are up-shifted and broadened compared to those for $\gamma_0 = 10$, showing the strong influence of the initial relativistic velocity of the electron on the spectrum [48]. The nearly single-cycle length of the NIR laser pulse causes further spectral broadening on figure 1, which makes them more different from those calculated earlier for the usual long laser pulses, especially when approximated by a continuous wave laser field [10, 45–47].

Based on these results, let us now consider the collective radiation of an attobunch of electrons, which consists typically of 10^5–10^8 electrons and has its longitudinal size ℓ in the 1–100 nm range. In particular, we use electron attobunch parameters based on the simulations of Naumova *et al* [26] and on the predictions of Sell and Kärtner [30]: it consists of $N = 10^8$ electrons with negligible energy spread, its distribution is uniform with a size of 800 nm ($=\lambda_L$) in the transverse direction, while its distribution is Gaussian with a size of 8 nm (6 standard deviation) in the longitudinal direction. Several experimental [24, 25, 31–34] and simulation results [49–51] suggest that these attobunch parameters are within reach experimentally in the near future.

Taking into account these parameters, the high intensity and the few fs length of the laser pulse, we may safely neglect the radiation reaction (the characteristic time of the energy loss by radiation reaction [18, 52] is 5 orders of magnitudes larger than the interaction time) and the electron–electron interaction (the Coulomb-force between the electrons is three orders of magnitude smaller than the Lorentz-force due to the laser pulse for $a_0 = 1$). The effect of the nonzero energy spread of the electron bunch can be estimated by changing the z-component of the beam velocity ($u^3(\theta_0)$) and comparing the resulting single electron spectra. These show that an energy spread of 0.1% causes a relative change in the spectral amplitude below 1% and a negligible change in the spectral phase. The nonzero transverse velocity components contribute to the nonzero transverse emittance of the attobunch via the divergence angle. However, the dominant terms of the trajectories (5)–(7) include only the longitudinal component of the velocity (i.e. $u^3(\theta)$). Additionally, the $\mathbf{n}$ for the essential part of emitted radiation is very close to the direction $\vartheta = \pi$ which further suppresses the effect of the transverse emittance in (18). These considerations thus justify to treat this attobunch as an ideal electron bunch, i.e. to neglect its energy spread and transverse emittance, the radiation reaction and the electron–electron interaction.

Then we can generalize equation (18) to describe the collectively emitted nonlinear Thomson-backscattered radiation of N electrons with the help of the coherence factor (sometimes called also relativistic form factor) [18, 36]:

$$C_N(\omega) = \sum_{k=1}^{N} \exp\left[\mathrm{i}\omega\left(t_k(\theta_0) - \frac{\mathbf{n}\cdot\mathbf{r}_k(\theta_0)}{c}\right)\right], \tag{19}$$

which takes into account the effect of the different initial positions of the electrons on the collectively emitted spectrum of N electrons as:

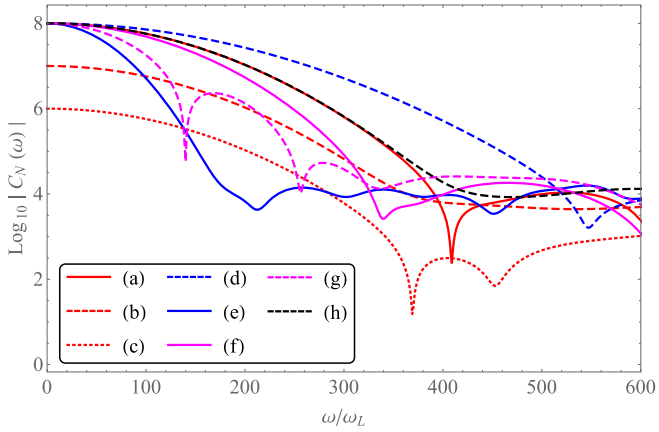

Figure 2. Magnitude of the coherence factor (19) for a particular random realization of the ideal electron attobunch described in the text. Parameters for curve (a): $N = 10^8$, $\gamma_0 = 10$, $\vartheta = 180°$, $\ell = 8$ nm. Parameter changes with respect to (a) for (b): $N = 10^7$; (c): $N = 10^6$; (d): $\ell = 15$ nm; (e): $\ell = 45$ nm; (f): $\vartheta = 179.8°$; (g): $\vartheta = 179.5°$; (h): $\gamma_0 = 15$.

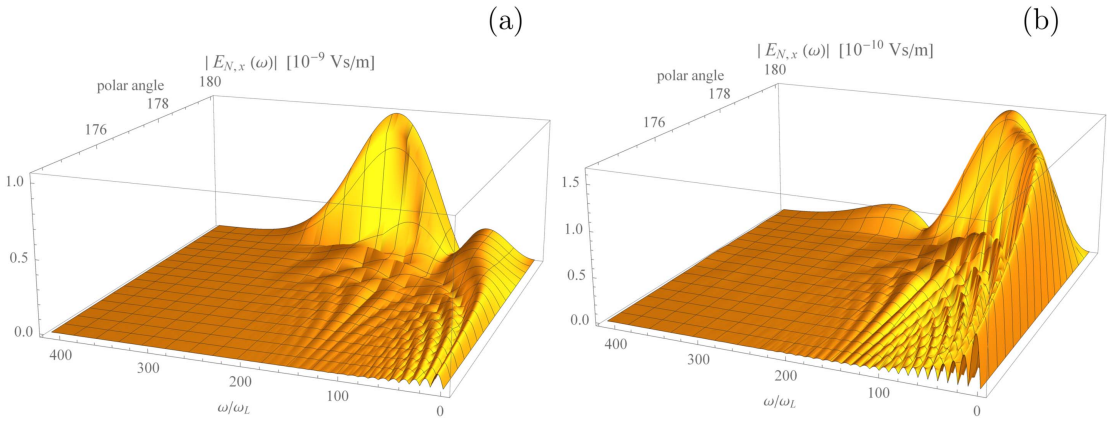

Figure 3. Polar angle dependence of the nonlinear Thomson-backscattering spectra, radiated collectively by an attobunch of 10^8 electrons, having an initial Lorentz factor of (a) $\gamma_0 = 10$ and (b) $\gamma_0 = 15$. We plot the spectra of the dominant x-component of the electric field, along the propagation directions in the x–z plane specified by the polar angles ϑ near the backscattering direction ($\vartheta = 180°$). Other parameters are the same as for figure 1.

$$\mathbf{E}_N(\omega) = C_N(\omega)\mathbf{E}_1(\omega). \tag{20}$$

The sensitive dependence of the coherence factor on certain parameters influences the collective radiation in a nontrivial way, therefore we examine first the magnitude of $C_N(\omega)$ in figure 2 on a logarithmic scale. For the attobunch parameters specified above, both the magnitude and the phase of $C_N(\omega)$ are independent of the particular set of individual electron coordinates at least up to the 400th harmonics. Although the shape of the curve (a) exhibits a slight fluctuation above this value, this does not influence the collective spectrum, since its magnitude is already negligible compared to its lower frequency values. Comparison of curves (a)–(c) clearly shows that the magnitude of the coherence factor scales linearly with the number of electrons, predicting the possibility of a superradiant collective emission. Note that the frequency range free of fluctuations slightly decreases with decreasing N. Comparison of curves (a), (d) and (e) shows that the frequency range of constructive coherent superposition is decreased inversely proportionally with the increasing longitudinal size of the attobunch. Comparison of curves (a), (f) and (g) shows that slight changes in the direction of the radiation have a very similar effect. However, curves (a) and (h) show, the coherence factor is not sensitive to the value of the initial Lorentz factor in this range.

Next we show the polar angle dependence of the spectral amplitude of the collective radiation in figure 3, computed on the basis of equation (20) for $\gamma_0 = 10$ in panel (a) and for $\gamma_0 = 15$ in panel (b). We plot the spectra of the dominant x-component of the electric field along the directions defined by the polar angles in the x–z plane. We set the polar angle range of these plots according to the usually expected beam divergence of $1/\gamma_0$, but we use this value with $\gamma_0 = 10$ in both panels for better comparison. It is clear from these plots that the angular range of the strongest high-frequency collective radiation is much more narrow then $1/\gamma_0$, especially for

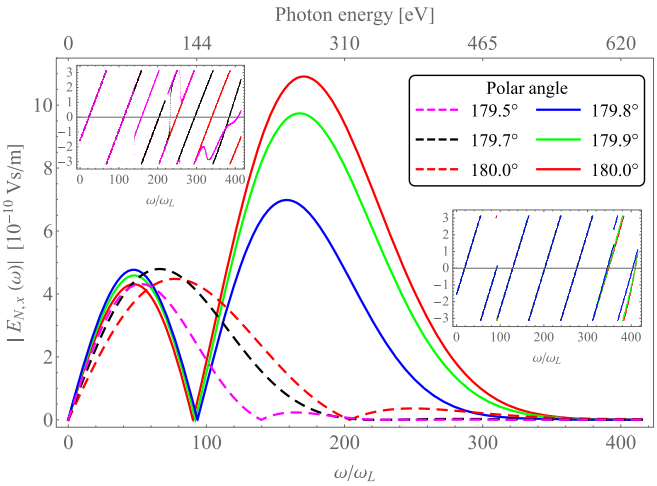

Figure 4. Nonlinear Thomson-backscattering spectra, radiated collectively by an attobunch of 10^8 electrons, having an initial Lorentz factor of $\gamma_0 = 10$ (solid line) and $\gamma_0 = 15$ (dashed line). We plot the spectra of the dominant x-component of the electric field, along the propagation directions in the $x-z$ plane specified by the polar angles in the legend. Other parameters are the same as for figure 1. The insets show the phases of the collective spectra in corresponding colors.

$\gamma_0 = 10$. Based on these plots, we selected two directions very close to $\vartheta = 180°$ for each of the values of γ_0 and we plot the spectra of the collective radiation along these ϑ directions in the $x-z$ plane in figure 4 for $\gamma_0 = 10$ (solid lines) and $\gamma_0 = 15$ (dashed lines). (Three of the single electron spectra in figure 1 are also along these directions.) Note that a considerable portion of this radiation is in the 2.33–4.37 nm (i.e. 283.7–532.1 eV) water window (especially for $\gamma_0 = 10$) which may provide an important possibility in the experimental study of organic molecules in water environment [53].

A comparison of figures 1 and 4 gives some surprising results: (seemingly) strongly reduced frequency range, a counter-intuitive dependence on γ_0, and extremely small divergence. In fact, all of these are explained by the coherence factor. The coherence factor 'amplifies' orders of magnitude stronger in the low-frequency part of the spectra than in their high-frequency part, which results in an apparent reduction of the frequency range of the spectrum. Nevertheless, the high-frequency part is still there, but much less amplified, i.e. with a negligible contribution to the collective radiation. This is most striking for $\gamma_0 = 15$: although the single electron spectra are shifted towards higher frequencies when changing from $\gamma_0 = 10$ to $\gamma_0 = 15$, this frequency range is already much less amplified by the coherence factor (which depends only weakly on γ_0), resulting a more red-shifted collective spectrum and considerably less radiated energy than in the case of $\gamma_0 = 10$. In other words, the single electron spectrum is better suited for the amplification by the coherence factor in the case of $\gamma_0 = 10$ than in the case of $\gamma_0 = 15$. Also in agreement with the sensitive dependence of $C_N(\omega)$ on the polar angle, the attobunch creates its collective radiation in a superradiant manner only in a narrow cone with an opening angle of a few tenth degrees, which results in a bright beam with an extremely small divergence compared to the usual case of nonlinear Thomson-backscattering. (We note that although the term superradiance was introduced in quantum optics for a process which involves also an interaction between the emitters mediated by the field [54], here we have independent emitters and we use the term superradiance only to emphasize that the intensity of the emitted radiation depends quadratically on the number of electrons in the bunch [55].) Comparing the curves along the polar angles $\vartheta = 179.9°$ and $\vartheta = 179.8°$ in the case of $\gamma_0 = 10$, and $\vartheta = 179.7°$ and $\vartheta = 179.5°$ in the case of $\gamma_0 = 15$, in figures 1 and 4, respectively, we see that the polar angle dependence of the coherence factor magnifies the slight difference of the single electron spectra and this way explains the extremely small beam divergence. In case of $\gamma_0 = 15$, unlike the expectation, the divergence of the emitted radiation does not decrease further but it is somewhat broader than for $\gamma_0 = 10$. Note also that for $\gamma_0 = 15$ the maximum of $|\mathbf{E}(\omega)|$ is not in the direction of the initial velocity of the electron bunch, as for $\gamma_0 = 10$.

The phase of the collective spectra, shown it the insets of figure 4, behaves very smoothly in the essential spectral range for both values of γ_0. Its dependence on the polar angles is almost negligible, i.e. it is within line width, which enables the synthesis of a narrow beam of attosecond pulses, to be discussed in the next section.

4. Properties of the emitted isolated attosecond pulses

We show the temporal pulse shapes of the collective radiation in figure 5, based on the inverse Fourier-transform of the corresponding collective spectra of figure 4. Remarkably, we have an isolated attosecond pulse for both of

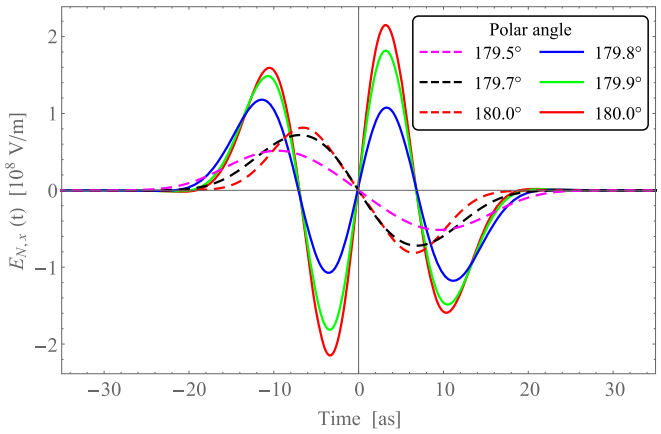

Figure 5. Temporal pulse shapes of the isolated attosecond pulses obtained by nonlinear Thomson-backscattering, computed from the spectra on figure 4, corresponding to $\gamma_0 = 10$ (solid line) and $\gamma_0 = 15$ (dashed line). We plot the dominant x-component of the electric field. Parameters are the same as for figure 1.

the values of γ_0, however, with different pulse shapes. Note also, that this pulse shape does not change considerably along the radiation directions with different polar angles and it is independent of the azimuthal angle, i.e. the pulse shapes are ca. the same within the beam spot.

For $\gamma_0 = 10$, the pulse has only two oscillations and its length at FWHM is 22.5 as. In a distance of $R_0 = 2$ m from the interaction region, the peak intensity is 6.14×10^9 W cm^{-2} and the average intensity is 1.81×10^9 W cm^{-2}, giving a pulse energy of 60.86 nJ. For $\gamma_0 = 15$, the pulse has only one single oscillation and its length at FWHM is 19.2 as. For $R_0 = 2$ m, the peak intensity is 9.68×10^8 W cm^{-2} and the average intensity is 5.55×10^8 W cm^{-2}, giving a pulse energy of 18.68 nJ. Although it may seem counter-intuitive that the bunch with higher γ_0 radiates a pulse with lower intensity and longer period, this follows from the collective spectra and is explained accordingly.

Regarding the polarization of the pulse, the x-component of the electric field is at least 3 orders of magnitude larger than its z-component. For nonzero values of the azimuthal angle, the radiation has also a y component which is similar in magnitude to the z-component. However, $E_{N,y}(t)$ is not in phase with the dominant x-component which makes the polarization of the pulse nontrivial around the nodes of the x-component. Nevertheless, this can be easily corrected for in an experiment if one wishes to have perfect linear polarization.

The above values of pulse energy and intensity are already high enough for state of the art pump–probe experiments. The quadratic dependence of these quantities on N in the superradiant parameter range may provide even larger values, if further increase in the number of electrons in the attobunch turns out to be feasible experimentally, but then the unavoidably increasing Coulomb repulsion between the electrons has to be taken into account.

Another way of increasing the pulse energy and intensity is to increase the intensity of the NIR pulse. We plot the temporal shapes of the resulting attosecond pulses at $\vartheta = 180°$ in figure 6, corresponding to a_0^2 values in the range of 4–12, and we plot the corresponding spectra in the inset. Here we assume a cosine-type NIR pulse and a longer electron attobunch with the parameters corresponding to curve (d) in figure 2. (Note also, that this longer electron attobunch generates lower intensity pulses than the one used in the case of figure 5.)

Based on the inset we see that, although the laser intensity is in the nonlinear regime, the collective spectra are actually the amplified linear peaks of the single electron spectra, due to the properties of the coherence factor. Since these peaks are also red-shifted and narrowed besides gaining more spectral intensity with increasing laser intensity, the resulting pulses get longer and have larger periods besides their increasing intensity.

In accordance with the spectra, the plots of figure 6 show that the intensity of the attosecond pulse increases nonlinearly with increasing NIR intensity up to a certain NIR intensity, while the pulse length increases only very moderately. E.g. for $a_0^2 = 10$, the pulse length is still not more than 45 as, but the peak intensity is already 1.31×10^{10} W cm^{-2} and the average intensity is 5.54×10^9 W cm^{-2}, giving a pulse energy of 381.69 nJ. These results suggest that there is an optimal NIR laser intensity for a given set of bunch parameters, which already yields the highest possible intensity of the attosecond pulse while its pulse length is still the shortest possible at that intensity. This feature is explained by effect of the increasing laser intensity on the single electron spectra: besides the red-shift there is slight narrowing and decrease of the (linear) peaks, which are, on the other hand, more strongly amplified by the coherence factor. The subtle interplay between these changes results in the dependence on laser intensity described above.

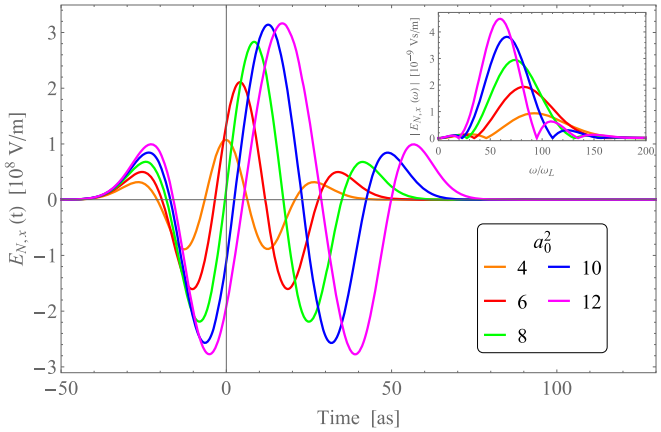

Figure 6. Temporal pulse shapes of the isolated attosecond pulses, obtained by nonlinear Thomson-backscattering at $\vartheta = 180°$, in case of the indicated values of a_0^2 for the NIR cosine-type ($\phi_0 = 0$) laser pulse. The inset shows the corresponding spectra. The electron bunch parameters correspond to curve (d) in figure 2.

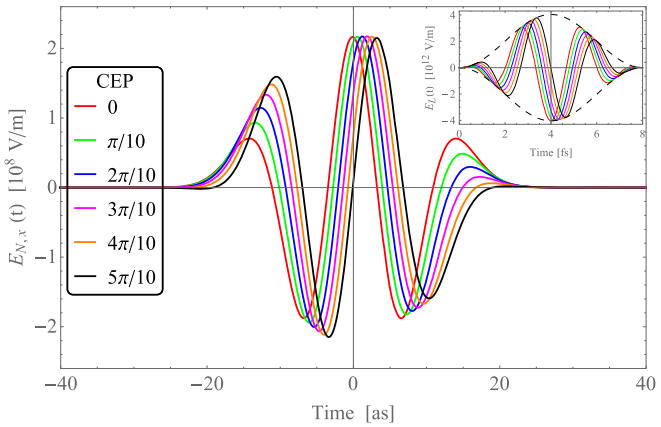

Figure 7. Temporal pulse shapes of the isolated attosecond pulses, obtained by nonlinear Thomson-backscattering at $\vartheta = 180°$, for different values of the CEP of NIR laser pulse given in the legend. The inset shows the pulse shapes of the incoming NIR pulses of different CEP with the corresponding colors. The $\gamma_0 = 10$, other parameters are the same as for figure 1.

Finally, we discuss the CEP dependence of the emitted attosecond pulses on the CEP of the single-cycle NIR laser pulse. Since this latter is an independent parameter in the solutions (5)–(7), it is straightforward to calculate the pulse shapes emitted by the attobunch for any value of the CEP of the NIR laser pulse. We show the results of this investigation in figure 7: the CEP of the attosecond pulse perfectly follows the CEP of the NIR laser pulse with a phase difference of π. This very simple relationship makes the CEP of these attosecond pulses easily controllable through the CEP of the NIR laser pulse, which is expected to have growing importance in attosecond pump and probe experiments.

5. Summary and conclusions

We have investigated the nonlinear Thomson-backscattering of a NIR laser pulse on an (ideally treated) relativistic electron bunch, based on an explicit analytic solution of the Newton–Lorentz equations which is valid for a frequently used laser pulse shape family. A suitable electron bunch, driven by a single-cycle laser pulse with and intensity corresponding to the nonlinear regime of Thomson scattering ($a_0 \geqslant 1$) radiates collectively in an extremely narrow beam. Our results show that an attobunch of 10^8 electrons having 5.2 MeV energy could produce an isolated XUV—soft x-ray pulse of 22.5 as length and 60.86 nJ energy, with its CEP locked to the CEP of the NIR laser pulse. Based on the analysis of the coherence factor, we also identified the important parameters of this superradiant process which may further enhance the pulse intensity. We found that the laser intensity can be increased up to an optimal value in the sense that the pulse intensity and energy increases nonlinearly but the pulse length increases only very moderately.

Our results may promote further theoretical and experimental research on XUV—soft x-ray pulse sources based on Thomson-backscattering, and on the generation of isolated electron attobunches.

Acknowledgments

The authors thank M G Benedict, P Földi, Zs Lécz, D Papp, Cs Tóth and Gy Tóth for stimulating discussions.

Funding

The project has been supported by the European Union, co-financed by the European Social Fund, EFOP-3.6.2-16-2017-00005. Partial support by the ELI-ALPS project is also acknowledged. The ELI-ALPS project (GOP-1.1.1-12/B-2012-000, GINOP-2.3.6-15-2015-00001) is supported by the European Union and co-financed by the European Regional Development Fund.

References

[1] Krausz F and Ivanov M 2009 *Rev. Mod. Phys.* **81** 163
[2] Baltuska A *et al* 2003 *Nature* **421** 611–5
[3] Goulielmakis E *et al* 2010 *Nature* **466** 739–43
[4] Krüger M, Schenk M and Hommelhoff P 2011 *Nature* **475** 78–81
[5] Peng L Y and Starace A F 2007 *Phys. Rev.* A **76** 043401
[6] Liu C, Reduzzi M, Trabattoni A, Sunilkumar A, Dubrouil A, Calegari F, Nisoli M and Sansone G 2013 *Phys. Rev. Lett.* **111** 123901
[7] Tibai Z, Tóth G, Mechler M I, Fülöp J A, Almási G and Hebling J 2014 *Phys. Rev. Lett.* **113** 104801
[8] Djiokap J M N, Hu S X, Jiang W C, Peng L Y and Starace A F 2012 *New J. Phys.* **14** 095010
[9] Ferrari F, Calegari F, Lucchini M, Vozzi C, Stagira S, Sansone G and Nisoli M 2010 *Nat. Photon.* **4** 875–9
[10] Esarey E, Ride S K and Sprangle P 1993 *Phys. Rev.* E **48** 3003
[11] Lee K, Cha Y H, Shin M S, Kim B H and Kim D 2003 *Phys. Rev.* E **67** 026502
[12] Yan W *et al* 2017 *Nat. Photon.* **11** 514–20
[13] Sarri G *et al* 2014 *Phys. Rev. Lett.* **113** 224801
[14] Khrennikov K, Wenz J, Buck A, Xu J, Heigoldt M, Veisz L and Karsch S 2015 *Phys. Rev. Lett.* **114** 195003
[15] Schoenlein R W, Leemans W P, Chin A H, Volfbeyn P, Glover T E, Balling P, Zolotorev M, Kim K J, Chattopadhyay S and Shank C V 1996 *Science* **274** 236
[16] Ta Phuoc K, Corde S, Thaury C, Malka V, Tafzi A, Goddet J P, Shah R C, Sebban S and Rousse A 2012 *Nat. Photon.* **6** 308–11
[17] Lau Y Y, He F, Umstadter D P and Kowalczyk R 2003 *Phys. Plasmas* **10** 2155–62
[18] Corde S, Ta Phuoc K, Lambert G, Fitour R, Malka V, Rousse A, Beck A and Lefebvre E 2013 *Rev. Mod. Phys.* **85** 1–48
[19] Kim D, Lee H, Chung S and Lee K 2009 *New J. Phys.* **11** 063050
[20] Chung S Y, Yoon M and Kim D E 2009 *Opt. Express* **17** 7853–61
[21] Luo W, Yu T P, Chen M, Song Y M, Zhu Z C, Ma Y Y and Zhuo H B 2014 *Opt. Express* **22** 32098–106
[22] Li J X, Hatsagortsyan K Z, Galow B J and Keitel C H 2015 *Phys. Rev. Lett.* **115** 204801
[23] Hack S, Varró S and Czirják A 2016 *Nucl. Instrum. Methods Phys. Res.* B **369** 45–9
[24] Geddes C G R, Toth C, van Tilborg J, Esarey E, Schroeder C B, Bruhwiler D, Nieter C, Cary J and Leemans W P 2004 *Nature* **431** 538–41
[25] Sears C M S *et al* 2008 *Phys. Rev. ST Accel. Beams* **11** 061301
[26] Naumova N, Sokolov I, Nees J, Maksimchuk A, Yanovsky V and Mourou G 2004 *Phys. Rev. Lett.* **93** 195003
[27] Esarey E, Schroeder C B and Leemans W P 2009 *Rev. Mod. Phys.* **81** 1229–80
[28] Maxson J, Cesar D, Calmasini G, Ody A, Musumeci P and Alesini D 2017 *Phys. Rev. Lett.* **118** 154802
[29] Zhu J, Assmann R W, Dohlus M, Dorda U and Marchetti B 2016 *Phys. Rev. ST Accel. Beams* **19** 054401
[30] Sell A and Kärtner F X 2014 *J. Phys. B: At. Mol. Opt. Phys.* **47** 015601
[31] Schmid K, Buck A, Sears C M S, Mikhailova J M, Tautz R, Herrmann D, Geissler M, Krausz F and Veisz L 2010 *Phys. Rev. ST Accel. Beams* **13** 091301
[32] Buck A, Nicolai M, Schmid K, Sears C M S, Sävert A, Mikhailova J M, Krausz F, Kaluza M C and Veisz L 2011 *Nat. Phys.* **7** 543
[33] Buck A *et al* 2013 *Phys. Rev. Lett.* **110** 185006
[34] Heigoldt M, Popp A, Khrennikov K, Wenz J, Chou S W, Karsch S, Bajlekov S I, Hooker S M and Schmidt B 2015 *Phys. Rev. ST Accel. Beams* **18** 121302
[35] Varró S and Farkas G 2008 *Laser Part. Beams* **26** 9–20
[36] Varró S and Ehlotzky F 1992 *Z. Phys.* D **22** 619–28
[37] Brau C A 2004 *Phys. Rev. ST Accel. Beams* **7** 020701
[38] Golovinski P A and Mikhin E A 2011 *J. Exp. Theor. Phys.* **113** 545–52
[39] Vais O E, Bochkarev S G and Bychenkov V Y 2016 *Plasma Phys. Rep.* **42** 818–33
[40] Sengupta N D 1949 *Bull. Math. Soc.* **41** 187
[41] McMillan E M 1950 *Phys. Rev.* **79** 498
[42] Goldman I I 1964 *Phys. Lett.* **8** 103
[43] Jackson J D 1999 *Classical Electrodynamics* 4th edn (New York: Wiley)
[44] Chen M, Esarey E, Geddes C G R, Schroeder C B, Plateau G R, Bulanov S S, Rykovanov S and Leemans W P 2013 *Phys. Rev. ST Accel. Beams* **16** 030701
[45] Hartemann F V, Troha A L, Luhmann N C and Toffano Z 1996 *Phys. Rev.* E **54** 2956–62
[46] Thomas A G R 2010 *Phys. Rev. ST Accel. Beams* **13** 020702

[47] Rykovanov S G, Geddes C G R, Vay J L, Schroeder C B, Esarey E and Leemans W P 2014 *J. Phys. B: At. Mol. Opt. Phys.* **47** 234013
[48] Salamin Y I, Mocken G R and Keitel C H 2003 *Phys. Rev.* E **67** 016501
[49] Kulagin V V, Cherepenin V A, Hur M S and Suk H 2007 *Phys. Rev. Lett.* **99** 124801
[50] Li F Y, Sheng Z M, Liu Y, Meyer-ter Vehn J, Mori W B, Lu W and Zhang J 2013 *Phys. Rev. Lett.* **110** 135002
[51] Wong L J, Freelon B, Rohwer T, Gedik N and Johnson S G 2015 *New J. Phys.* **17** 013051
[52] Landau L and Lifshitz E 1975 The classical theory of fields *Course of Theoretical Physics* vol 2 4th edn (Oxford: Pergamon)
[53] Nisoli M, Decleva P, Calegari F, Palacios A and Martin F 2017 *Chem. Rev.* **117** 10760–825
[54] Dicke R H 1954 *Phys. Rev.* **93** 99–110
[55] Schott G A 1912 *Electromagnetic Radiation* (Cambridge: Cambridge University Press)